

PCCP

Accepted Manuscript



This is an *Accepted Manuscript*, which has been through the Royal Society of Chemistry peer review process and has been accepted for publication.

Accepted Manuscripts are published online shortly after acceptance, before technical editing, formatting and proof reading. Using this free service, authors can make their results available to the community, in citable form, before we publish the edited article. We will replace this *Accepted Manuscript* with the edited and formatted *Advance Article* as soon as it is available.

You can find more information about *Accepted Manuscripts* in the [Information for Authors](#).

Please note that technical editing may introduce minor changes to the text and/or graphics, which may alter content. The journal's standard [Terms & Conditions](#) and the [Ethical guidelines](#) still apply. In no event shall the Royal Society of Chemistry be held responsible for any errors or omissions in this *Accepted Manuscript* or any consequences arising from the use of any information it contains.

Optical and surface enhanced Raman scattering properties of Au nanoparticles embedded in and located on a carbonaceous matrix

Jai Prakash^{1*}, Vinod Kumar¹, R. E. Kroon¹, K. Asokan², V. Rigato³, K. H. Chae⁴, S. Gautam⁴, H. C. Swart¹

¹Department of Physics, University of the Free State, Bloemfontein, ZA 9300, South Africa

²Inter University Accelerator Centre, Aruna Asif Ali Marg, New Delhi 110067, India

³INFN Laboratori Nazionali di Legnaro, Via Romea. 4, 35020 Legnaro, Padova, Italy

⁴Advanced Analysis Center, Korea Institute of Science and Technology, Seoul 136-791, Republic of Korea

***Corresponding author: Jai Prakash**

Email: jai.gupta1983@gmail.com, prakashJ@ufs.ac.za

Abstract

Au nanoparticles (NPs) on the surface and embedded in a matrix have been the subject of studies dealing with a variety of spectroscopic and sensing applications. Here, we report on low energy Ar ion induced evolution of the morphology of a thin Au film on a polyethyleneterephthalate (PET) substrate along with thermodynamic interpretations, corresponding unique surface plasmon resonance (SPR) and photoluminescence (PL) properties. These properties are linked to the variation of surface nanostructures and surface enhanced Raman scattering (SERS) effect of methyl orange (MO) dye adsorbed on the surface. Ion induced thermal spike and sputtering resulted in dewetting of the film with subsequent formation of spherical NPs. This was followed by embedding of the NPs in the modified PET due to thermodynamic driving forces involved. The surface and interface morphologies were studied using atomic force microscopy and cross-sectional transmission electron microscopy. X-ray photoelectron spectroscopy was used to study the chemical changes in the system upon irradiation. The optical properties were studied by diffuse reflectance UV–vis spectroscopy and PL using a 325 nm He-Cd laser. The red shift of the SPR absorption and blue shift of the PL emission have been correlated with the surface morphology. The blue PL emission bands around 3.0 eV are in good agreement with the literature in respect to the morphology changes and the blue shift is attributed to compressive strain on the embedded Au NPs. Enhancement of the SERS signals is observed and found to be correlated with the SPR response of the Au nanostructures. The SERS analyses indicate that MO molecules may be adsorbed with different orientations on these surfaces i.e. Au NPs located on the surface or embedded in the modified PET. These polymeric substrates modified by NPs can have a potential application in solid-state light emitting devices and can be applied in SERS based sensors for the detection of organic compounds.

1. Introduction

Noble metal nanoparticles (NPs) that are embedded in and located on the surface of insulating materials such as polymers and glass forming nanocomposites have been shown to have unique physical properties. These properties make them potential candidates for optical, electrical and other applications [1-5]. Because of their low dielectric constant, in addition to their easy processing and low cost production, polymers are attractive as host materials for the synthesis of nanocomposites containing metal NPs. Therefore, polymer based composite materials embedded with noble metal NPs have been the subject of great interest for the fabrication of optically active media and futuristic nano-electronics devices [6,7]. When such a system is excited by light, photons are coupled to the metal-dielectric interface and a strong absorption maximum at a particular wavelength in the UV-visible region is then observed due to a photon induced oscillation of the electron charge density. This is called the surface plasmon resonance (SPR) wavelength [7,8]. This phenomenon of SPR influences the excited state properties of materials and improves the performance of organic and inorganic based electronic devices. For example: noble metal NPs were found to effectively enhance the performance of polymer based solar cells and light emitting diodes [9,10]. Similarly, Nakayama et al. [11] have reported an improvement in efficiency of an optically thin GaAs solar cell decorated with size-controlled Ag NPs. The emission of noble metals is also interesting with respect to its origin and for its application in sensing, optoelectronic [12,13] and electroluminescence devices i.e. in the use of Au as a semi-transparent electrode [14]. The weak fluorescence of bulk noble metals was first discovered by Mooradian [15] and later, visible photoluminescence (PL) from Au NPs, was discovered by Wilcoxon et al. [16]. Recent advances in nanotechnology have revealed that the NPs have enhanced fluorescence emission compared to the bulk metals [17,18]. Broad red luminescence

has been observed from an ultrathin Au film and ascribed to the radiative decay of collective plasmon states of the Au nano-islands [14,19]. Fluorescence of Au NPs has been investigated extensively including quantum yields, lifetimes and it has been shown that the emission is highly tuneable by small changes in the particle size [18,20]. White PL has been reported in Au NPs, extremely useful for biological and medical applications such as *in vivo* imaging, because of the transparency and reduced cell damage of human and animal tissues in the near infrared spectral range [2,21]. Eichelbaum et al [2] have studied three-photon-induced white PL from Au NPs embedded in and located on the surface of glassy silicate-titanate layer produced by annealing and NIR femtosecond laser irradiation. Au NPs have been shown to have potential applications in sensors based on surface enhanced Raman scattering (SERS) and are a powerful alternative to organic and inorganic luminescence markers [2]. SERS involves a dramatic enhancement of the intensity of Raman scattering from molecules adsorbed on or in proximity to a nanostructured metal surface as a result of strong local electromagnetic field enhancement [22]. Both SPR and SERS have been widely investigated using noble metal NPs (Ag, Au) in solution and on substrates for highly sensitive label-free chemical and biological sensors [2, 22-26].

The performance of a device (based on NPs or their nanocomposite materials) can be controlled by tuning the position of the SPR and PL wavelengths, their band width and intensity etc. These depend on shape, size, interparticle separation and spatial distribution of NPs as well as the surrounding dielectric medium [8,27]. Although, several chemical and litho-graphical methodologies have been developed to synthesize NPs with tunable size and shapes, the synthesis of NPs embedded in thin films with a desired shape and size for functional properties is not simple. This is because of the minimization of surface energy criterion for stability of nanostructures which is a minimum for the spherical shaped NPs [28]. The synthesis of such a

noble metal NP-polymer system and the ability to control the structure of such assemblies in order to improve the performance is therefore an important aspect of investigation both from the fundamental and technological aspects. Ion beam techniques have been found to be one of the possible methods for the synthesis of NPs of different shapes and sizes that can be embedded at a desired depth in a substrate [28]. For instance, 100 keV Ar ion irradiation induced mixing of Au films on SiO₂ [12] resulted in embedded Au NPs in SiO₂ matrix and produced strong SPR and broad blue luminescence. Metal NPs embedded in and positioned on the top of the substrates have been reported using ion beam induced mixing technique for various energy regimes [29,30-35].

Among noble metals, Au is one of the most preferred materials because of the large enhancement of the local field provided under irradiation in the visible and NIR as well as its high stability and biocompatibility [36]. Recently, we have reported the synthesis of Au NPs on the surface and embedded in carbonaceous matrix using 150 keV Ar ion irradiation of a Au/polyethyleneterephthalate (PET) bilayer system. The ion irradiation induced thermal spikes resulting from collision cascade and produced molten zones which lead to dewetting and nanopatterning through sputtering and interface mixing [29]. In addition, we have also modelled the mechanism of the embedding processes of Au NPs based on the thermodynamic driving forces related to the surface and interface energies of the metal NPs and polymer surfaces [30]. In the present study, we have investigated the irradiation induced dependence of morphological evolution of a thin Au film on PET due to 150 keV Ar ion irradiation at various fluences ranging from 5×10^{15} to 5×10^{16} ions/cm² and the corresponding unique variation of the SPR and PL properties. The SERS effect of methyl orange (MO) adsorbed on these irradiated surfaces has also been investigated. The morphology evolution was characterized using Rutherford

backscattering spectrometry (RBS) and high resolution imaging techniques namely AFM for surface and cross sectional-TEM for interface analysis. The optical response was measured using UV–vis spectroscopy and PL excited by a 325 nm He-Cd laser. X-ray photoelectron spectroscopy (XPS) was carried out to investigate the chemical changes on the surface. SERS signals were detected using an NXR FT-Raman module microscopy system. The correlation between the evolution of the surface morphology and the optical properties as well as SERS effect was established in terms of the corresponding thermodynamic driving forces.

2. Experimental details

2.1 Thin Au film deposition on PET substrate and ion beam irradiation: Thin Au films (15 nm) on PET were deposited by electron beam evaporation in an ultra-high vacuum chamber (base pressure of 10^{-5} Pa). These bilayer systems were irradiated with 150 keV Ar ions at fluences ranging from 5×10^{15} to 5×10^{16} ions/cm². Ion beam energy was chosen on the basis of range and energy loss calculations using (stopping and range of ions in matter) SRIM-2008 to ensure that the maximum of damage profile occurred at the interface. More details about the sample preparation and ion beam parameters are described elsewhere [29]. The film thickness and ion induced sputtering yield of irradiated samples were estimated from RBS spectra using Rutherford universal manipulation programme (RUMP) simulation software.

2.2. UV–Vis spectroscopy: UV-Vis diffuse reflectance measurements were carried out in air in the wavelength range 250-800 nm using Lambda 950 UV–Vis-NIR spectrophotometer with integrating sphere from PerkinElmer. A baseline correction was implemented prior to the measurement and spectralon was used as a standard. A dip in reflectance spectra was observed at around 500 nm due to the SPR band of Au NPs produced after ion irradiation.

2.3. PL study: PL measurements were carried out at room temperature using a He-Cd laser emitting at 325 nm to excite the samples. A iHR320 spectrometer from Horiba was used to analyse the luminescence which was measured using a thermoelectrically cooled R928 photomultiplier tube from Hamamatsu.

2.4. Atomic force microscopy (AFM): Morphological analysis and surface roughness of the samples before and after irradiation were carried out by using Nanoscope IIIa multimode SPM with an antimony-doped silicon tip in tapping mode.

2.5. Cross-section transmission electron microscopy (X-TEM): X-TEM measurements were carried out using FEI, Tecnai F20 G² TEM at 200 kV to characterize thin Au film, Au NPs at interface and embedded Au NPs in the substrate as well as their distribution.

2.6. X-ray diffraction (XRD): Samples were characterized using a Bruker D8 X-ray diffractometer operating at 40 kV and 40 mA using Cu K α X-rays with wavelength 0.15406 nm and a scan range of 20°–80°.

2.7. X-ray photoelectron spectroscopy (XPS): The samples were investigated by XPS to study the chemical changes on the surface after ion beam irradiation. The experiments were carried out in the UHV system with a base pressure of 5×10^{-11} mbar. A monochromatized Mg K α X-ray source was used with an acceleration voltage of 13 kV and an emission current of 10 mA. High-resolution scans were carried out with a pass energy of 50 eV, dwell time of 0.1 s and a step size of 0.05 eV. The C 1s peak at 284.4 eV was used as the reference energy for correction of the energy scale due to charging.

2.9. Sample preparation and characterisation for SERS study: In order to investigate the effectiveness of the prepared films with Au nanostructures for the detection organic dye molecule MO, the substrates were immersed in an aqueous solution of MO (400 mM) for 1-2 h

for the adsorption process to occur and then allowed to dry. The dye powder was used as received without any further purification. Raman spectra were measured for the MO powder as well as for aqueous solutions of MO on the uncoated PET polymer, as-prepared Au-coated PET film and irradiated Au-coated PET films. The SERS signals were detected using an NXR FT-Raman module microscopy system with 2.5 W Nd:YVO₄ laser excitation of 1064 nm wavelength and a high-performance liquid nitrogen-cooled germanium detector.

3. Results and discussion

3.1 Formation of Au NPs on surface and embedding into substrate

Cross-sectional TEM images of the as deposited thin Au film on PET and films irradiated by 150 keV Ar ions at different fluences of 5×10^{15} , 1×10^{16} , and 5×10^{16} ions/cm² are shown in Figure 1. The unirradiated thin Au film is smooth with small and insignificant features on the surface. After irradiation at a fluence of 5×10^{15} ions/cm² the Au film dewets from the substrate and connected patterned nanostructures such as nanospheroids are formed on the surface. The dewetting of thin metallic films on various substrates has been reported under ion bombardment [29,30,35,37]. The dewetting mechanism of the thin Au film on PET has already been discussed in detail in ref [29]. Induced thermal spikes are produced by Ar ions due to collision cascades, creating nanometer size molten zones in the Au film. The maximum size of the molten zones leading to dewetting of the Au film was estimated to be about 3 nm from the expression [1,29] $r_m^0 = (E_d^0 / \pi n_0 \epsilon_m)^{1/2}$, where, E_d^0 is the deposited energy per unit length by an ion along its path, n_0 is the atomic density of metal and $\epsilon_m (\approx 3kT_m)$ is the average energy of the atom at the melting temperature (T_m). Craters are formed on the Au film as a result of the sputtered outflow of the Au atoms from the hot molten zones [29,30,35,38].

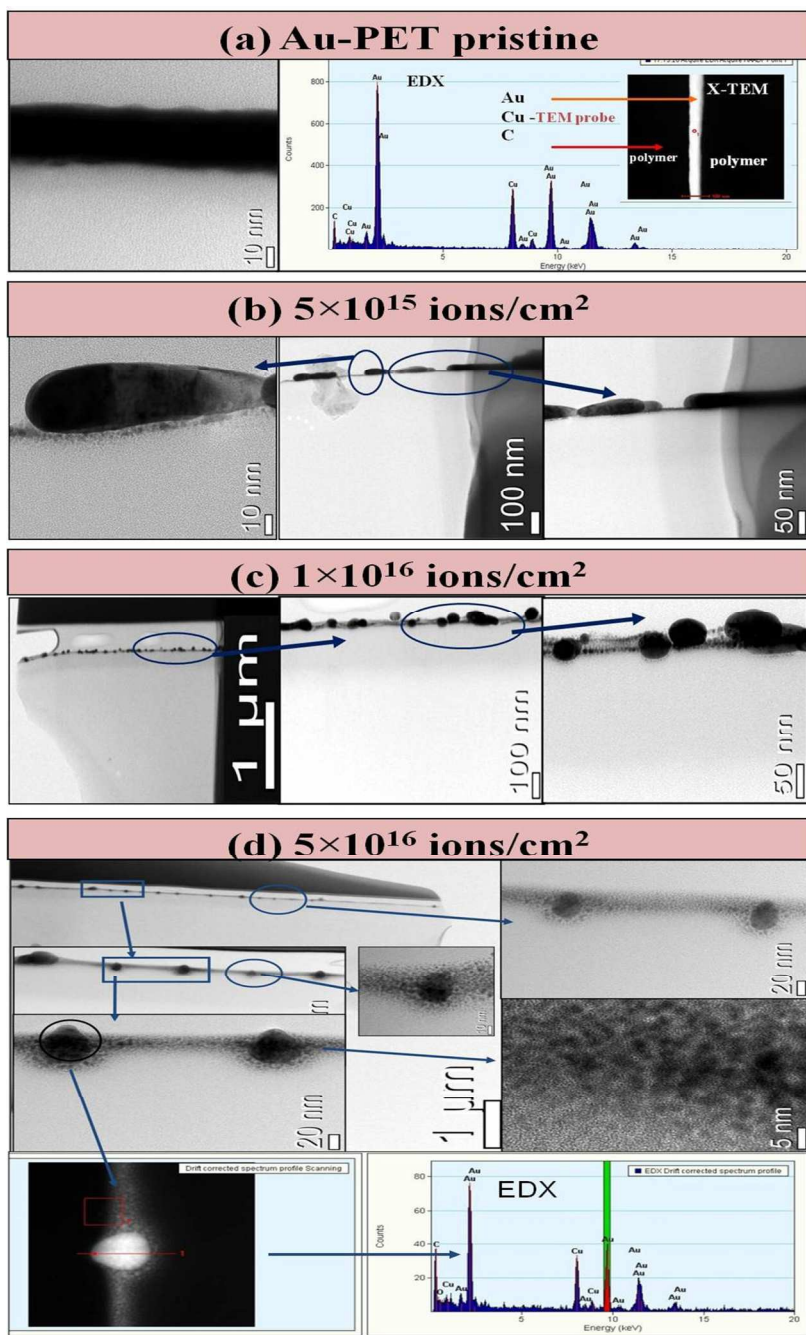


Figure 1: X-TEM images of (a) as deposited Au film on PET (with EDX) and films after 150 keVAr ion irradiation at fluences of (b) 5×10^{15} , (c) 1×10^{16} , and (d) 5×10^{16} ions/cm² (with EDX of one of Au nanoparticles partially embedded in matrix). [Figures in partial have been reproduced from the source: Jai Prakash et al., Synthesis of Au nanoparticles at the surface and embedded in carbonaceous matrix by 150 keVAr ion irradiation, J. Phys. D: Appl. Phys 44, 125302 (2011) with permission from IOP publishing Ltd., Bristol]. [Figures in partial have also been taken from

source Prakash et al, Phenomenological understanding of dewetting and embedding of noble metal nanoparticles in thin films induced by ion irradiation”*Mat. Chem. Phys* 2014; 147 (3): 920-924. Copyright (2014), with permission from Elsevier]

The higher surface energy of the Au film as compared to the polymer surface (because of the high cohesive energy of the metals) also promotes crater formation which contributes to dewetting [30,39]. The irradiation also induces chemical alterations in the PET as a result of bond breaking and the release of hydrocarbons forms a carbon rich modified polymer layer near the interface [29]. With an increase in ion fluence, AFM micrographs (Figure S1) show partially connected nanostructures for a fluence of 1×10^{16} , and isolated Au NPs located in a carbonaceous matrix for a fluence of 5×10^{16} ions/cm² respectively. When examined with X-TEM, it was found that for a fluence of 1×10^{16} ions/cm², the partially connected nanostructures (as observed by AFM) are actually spherical Au NPs positioned on the surface, whereas for a fluence of 5×10^{16} ions/cm² these NPs become fully or partially embedded into the carbonaceous matrix surrounded by very small Au NPs (less than or equal to 5nm) near the surface region (Figure 1d). There is an embedding force for NPs positioned at the surface. This arises from the higher surface energy of the metal NPs compared to the polymer and their thermodynamic instability on dielectric surfaces. The thermodynamic driving force for the embedding of the NPs originates from the tendency of the system to reduce this surface energy [30,40.]. It was shown in a previous publication [30] that the thermodynamic driving force favours the embedding of Au NPs in a modified PET surface which satisfies the condition $\gamma_{NP} > (\gamma_{polymer}) + (\gamma_{NP-polymer})$, where, γ_{NP} is the surface energy of the NPs, $\gamma_{polymer}$ is the surface energy of the substrate and $\gamma_{NP-polymer}$ is the interfacial energy. This interfacial energy was calculated using $\gamma_{Au NP-PET} = \gamma_{PET} - \gamma_{Au NP} \cdot \cos$

θ_{cont} , where $\gamma_{\text{Au NP-PET}}$ is the interfacial energy between a Au NP and the polymer, γ_{PET} is the surface energy of the PET, $\gamma_{\text{Au NP}}$ is the surface energy of the Au NP and θ_{cont} is the contact angle of the Au NP with the PET surface. It was found that the surface energy of the Au NPs is greater than that of the estimated interfacial energy $\gamma_{\text{Au NP-PET}}$ and hence embedding was energetically favorable. More details about these calculations can be found in ref. [30]. EDX was performed to confirm the presence of Au NPs as well as the mixed carbon rich region embedded with Au NPs after irradiation at a fluence of 5×10^{16} ions/cm² as shown in Figure 1d, and also confirmed by SEM/EDX as reported in ref. [29]. The surface roughness was measured with an AFM in tapping mode for the unirradiated and irradiated samples. The surface roughness increases from 2 nm (pristine) to 7 nm with increasing fluence up to 1×10^{16} ions/cm² because of discontinuous Au film and the formation of percolated grains as a result of irradiation induced dewetting and sputtering. The surface becomes slightly smoother at the higher fluence of 5×10^{16} ions/cm² with isolated and spherical Au NPs on the surface due to sputtering and diffusion of Au in the polymer as shown in figure S1 (supplementary data). The sputtering of the Au film was estimated by calculating the areal density of the Au extracted from the RBS spectra as reported in ref. [29] and it was found that the areal density decreases with increasing ion fluence. Overall, we have demonstrated that the sputtering of the thin Au film and the strong tendency of the noble metals to aggregate on the polymer surface (because of their high cohesive energy along with ion induced thermal spikes) leads to dewetting of the film followed by NP formation on the ion modified PET surface. The formed Au NPs that have a surface energy greater than the estimated interfacial energy of the NPs and polymer get embedded into the modified polymer surface with

further irradiation due to the thermodynamic (capillary) driving forces and ion induced viscous flow in the polymer [30].

3.2 Chemical alterations in the Au/PET system induced by ion irradiation

The observations based on RBS, AFM/SEM and TEM analyses show nanostructuring of the thin Au film through dewetting and NPs formation on the surface, followed by embedding of the NPs into the surface. The presence of Au NPs is again confirmed by XPS and an analysis of core levels was carried out to investigate the distribution of NPs and ion induced chemical alterations in the system.

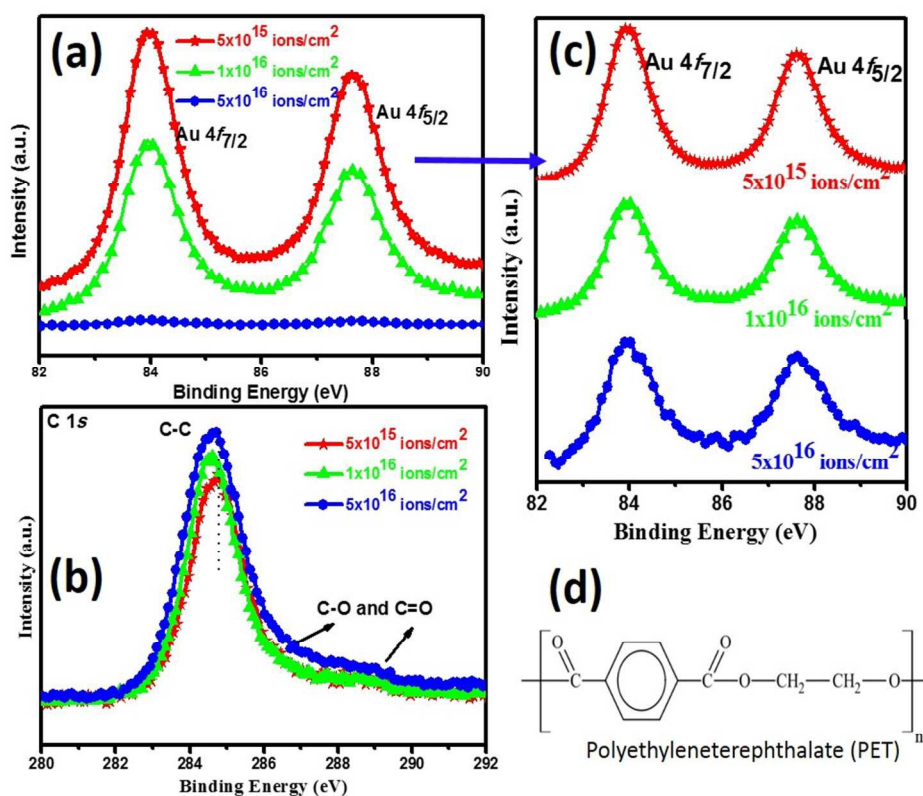


Figure 2: (a) Au $4f_{7/2}$ and $4f_{5/2}$ core levels of the photoemission spectra for Au-PET samples irradiated with 150 keV Ar ions for the fluences of 5×10^{15} , 1×10^{16} and 5×10^{16} ions/cm². (b) C 1s core levels of the photoemission spectra for Au-PET samples irradiated with 150 keV Ar ions for

the fluences of 5×10^{15} , 1×10^{16} and 5×10^{16} ions/cm². (c) Normalized photoemission spectra of Au $4f_{7/2}$ and $4f_{5/2}$ core levels for Au-PET at each ion fluence showing the broadening and asymmetric tailing of the peaks at the higher fluences. (d) Chemical structure of PET indicating presence of various elements and bondings.

Figure 2 (a) shows the Au $4f_{7/2}$ and $4f_{5/2}$ core levels of the photoemission spectra, which have been recorded for the Au-PET samples irradiated with 150 keV Ar ions for the fluences of 5×10^{15} , 1×10^{16} and 5×10^{16} ions/cm². Note that the photoemission spectra for the pristine Au-PET sample is almost identical to the one irradiated at 5×10^{15} ions/cm² except for the change in intensity because of the sputtering of Au and is not shown here. The normalized $4f$ peaks for each ion fluence are shown in figure 2(c).

For the photoemission spectra three aspects have been taken into consideration, namely the (i) intensity, (ii) position, and (iii) full width at half maximum (FWHM) of the Au $4f_{7/2}$ and $4f_{5/2}$ peaks. The peak intensity clearly decreases with increased irradiation fluence. The decreased intensity can be understood by the sputtering of Au by the 150 keV Ar ions, as also revealed by the RBS measurements and the surface morphology of irradiated samples. There is a very small shift of 0.02 eV and ~ 0.06 eV in the peak positions of Au $4f_{7/2}$ and $4f_{5/2}$ after irradiation fluence of 1×10^{16} and 5×10^{16} ions/cm² respectively, which indicates that there is no chemical reaction of the Au, since generally, a shift could be due to the influence of the surrounding environment [41]. It is also confirmed by the C 1s core level photoemission spectra shown in figure 2(c) that there is no indication of Au-C interaction. (It is also to be noted that Au solubility in C is only 8.2×10^{-6} at. % [41]). Similar binding energy shifts around ~ 0.3 eV in the position of the Au $4f_{7/2}$ (84.0 eV) and $4f_{5/2}$ (87.6 eV) peaks have been observed in the case of the Au-SiO₂ system [42] and of 0.6 eV in the case of embedded Au NPs in glassy carbon [43], with no indication of

any Au-O or Au-C bonds. The shift in binding energy has also been shown to depend on the size of Au NPs. Binding energy shifts of 0.15 eV and 0.3 eV have been reported for the particle size less than or equal to 2 nm and 1 nm, respectively [44]. On the contrary, in our case the shift in binding energy is very small, indicating larger particles (greater than 10 nm) and a large size distribution with smaller NPs of less than or equal to 5 nm at the fluence of $\times 10^{16}$ and 5×10^{16} ions/cm² respectively. Concerning the FWHM broadening of the peaks and shape, there are several contributions to be taken into account. It can be observed that the FWHM of the peaks is increased by 0.1 eV and 0.6 eV after ion irradiation fluences of 1×10^{16} and 5×10^{16} ions/cm² respectively. It has been reported that broadening in photoemission spectra increases with a decrease in the particle size [43,44] since the change in the binding energy (ΔE) depends on the size (d) of the NPs according to the expression [41] $\Delta E = 1/4\pi\epsilon_0\epsilon \cdot (e^2/d)$, where, e is the electron charge, ϵ_0 is the vacuum dielectric function and ϵ is the relative dielectric function of the medium surrounding the clusters. The broadening observed in photoemission spectra of samples irradiated at fluences of 1×10^{16} and 5×10^{16} ions/cm² is due to a decrease in the size of the NPs as also observed in the TEM results. For the sample irradiated at the fluence of 5×10^{16} ions/cm², the broadening is also accompanied by an asymmetric line shape because of the development of a high binding energy tail. It can be understood by the 1/d dependence of the binding energy as mentioned in the above expression, which indicates the presence of the smaller Au NPs with various sizes [41,43,44], which is in good agreement with TEM results in the present case.

The C 1s core level photoemission spectra were also studied to understand the ion induced effect in the polymer layer near the interface. Figure 2(b) shows the C 1s core level photoemission for the Au-PET samples irradiated with 150 keV Ar ions at the fluences of 5×10^{15} , 1×10^{16} and 5×10^{16} ions/cm². A prominent C1s peak at 284.8 eV corresponds to C-C

bonds is considered as a reference peak. With increasing ion fluence, the peak intensity increases with a small shift towards lower binding energy, which can be understood by the fact that the evolution of various hydrocarbons and the loss of hydrogen with increasing ion fluence leads to graphitization and carbonization [45]. Similarly, several types of chemical reaction have been observed to occur in the case of polymers exposed to ion irradiation, such as dehydrogenation, loss of oxygen, loss of aromaticity via ring opening [46,47]. Along with an increase in the intensity of C-C peak, it is also observed that with increasing fluence other components such as C-O and C=O appeared at about 286 eV and 289 eV, respectively [48]. This indicates that the fraction of polymer surface area is increased with increasing ion fluence and the surface becomes carbon rich with PET components [figure 2(d)] at the highest fluence, which is in agreement with RBS, SEM and EDX results.

3.3. Optical properties of Au NPs located at the surface and embedded in the Matrix

UV-Vis spectroscopy results

The presence of nanoscale metallic particles of Au in the ion-beam irradiated samples has been examined further through optical absorption spectroscopy measurements. As shown in Figure 3, the characteristic SPR band (the minimum reflectance located at the dip of the reflectance spectra) of Au NPs have developed with increasing Ar ion irradiation fluence. The as-deposited (pristine) Au film does not show any characteristic SPR band (i.e. no dip in the reflectance spectrum) whereas for irradiated samples the dip around 500 nm (~ 2.5 eV) is attributed to the SPR absorption of Au NPs [12]. For the sample irradiated with 5×10^{15} ions/cm², we observed enlarged NPs that form a connected nanostructure with an open polymer area fraction (Figure 1(b)). The SPR band of the Au NPs matches closely with that reported for these type of interconnected irregular shaped Au nanostructures [49]. On further increasing the ion fluence,

spherical Au NPs are formed (Figure 1(c)) and surface plasmons in the structures become localized, which results in a strong SPR band at 498 nm as seen in the reflectance spectrum of the sample irradiated with a fluence of 1×10^{16} ions/cm² (Figure 3). The resonance band in the reflectance spectra decreased significantly for the sample irradiated at the fluence of 5×10^{16} ions/cm² for which completely or partially embedded Au NPs are formed (Figure 1(d)).

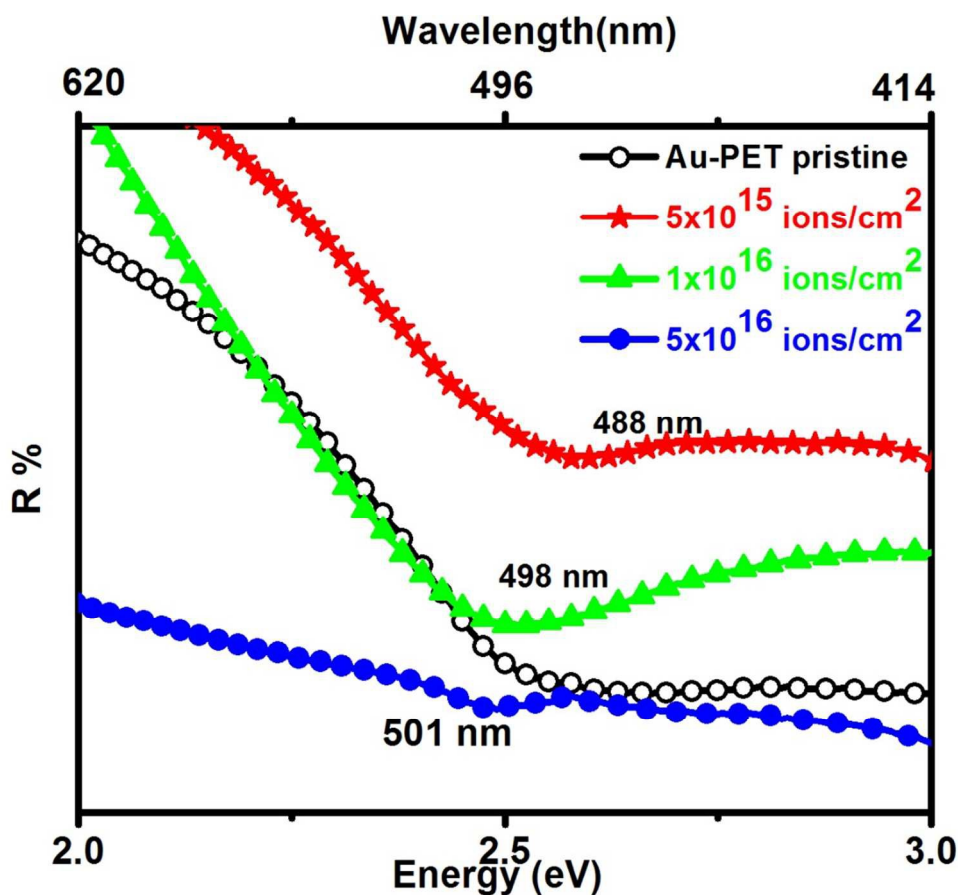


Figure 3: UV-Vis diffuse reflectance spectra of as deposited Au film on PET and the films after 150 keV Ar ion irradiation at fluences of 5×10^{15} , 1×10^{16} , and 5×10^{16} ions/cm².

Interestingly, there is a red shift of the resonance peak position with an increase in ion fluence, along with the change in shape and size of the Au nanostructures. Several authors have reported on the effect of size, shape, and density of NPs and their surrounding media on the

width and position of the plasmonic peaks [28,49-51]. The UV-Vis reflectance spectrum of the sample irradiated with 5×10^{15} ions/cm² revealed an absorption peak at 488 nm consistent with plasmonic resonance of spheroid Au nanostructures and nanorods. Nanorods generally show two plasmonic resonance bands, with the shorter wavelength absorption band corresponding to resonance perpendicular to the major axis (transverse plasmon band) and the longer wavelength absorption band being related to resonance along the major axis (longitudinal plasmon band) [50,52]. The plasmonic peak positions may be shifted either longer or shorter depending on the ratio between the lengths of the two axes. In the present case the observed SPR band in the reflectance spectrum for spheroid Au nanostructures formed with the fluence of 5×10^{15} ions/cm² did not show this two band behaviour. Similar results were also presented by Gaspar et al. [49] in the case of Au spheroid NPs obtained by depositing thin Au layers on glass substrates. They observed a red shift in the plasmon band position when spheroid structures were formed from spherical Au NPs and explained that the red shift may have equal contribution of both transversal and longitudinal enlargement of the NPs. Similarly, Sun et al. [53] have reported the correlation between the thin Au film morphology evolution (for varying annealing temperature) and surface plasmon absorption. They observed that a thin deposited film has a porous-like interconnected island structure which, after annealing (200-400 °C), tends to spheroid-like NPs. At higher annealing temperatures (400-700°C) spherical NPs are formed. In this case reflectance spectra for the spheroid nanostructures also only exhibited a single SPR band, because the majority of the spheroids had an isotropic shape with aspect ratio less than 2.0. In the current study, we observed similar spheroid shaped Au NPs after a fluence of 5×10^{15} ions/cm² with only one surface plasmon band that is attributed to small connected spheroid NPs. When two NPs are close to each other, there is the possibility of plasmonic dimer formation with a corresponding

red shift which depends on the interaction distance between the NPs [49]. A red shift in the surface plasmon band of the Au NPs was observed because of interparticle coupling when NPs are close to each other as compared to when particles are separated [49]. Sun et al. [53] explained a blue shift of the surface plasmon band position by an increase of the average separation between nanostructures, resulting in a weakening of the coupling effect. On the contrary, in our case Au spheroid NPs change their shape into more regular and spherical NPs upon ion induced thermal-dewetting and sputtering, thus decreasing the area of the spheroid nanostructures and giving rise to a red shift. This red shift (10 nm) may be due to the strong interparticle coupling effect of isolated but densely distributed spherical Au NPs [27,49], which is consistent with the Au NPs distribution as observed in cross-sectional TEM images for the fluence of 1×10^{16} ions/cm² (Figure 1(c)). The reflectance spectra reveal a further red shift (from 498 to 501 nm) in the Au surface plasmon band between the fluences of 5×10^{16} and 5×10^{16} ions/cm² respectively, with an increase in the FWHM when embedded Au NPs are formed in the carbonaceous matrix (Figure 1(d)). As mentioned above, there are many other factors that may affect the surface plasmon band position and that can lead to a red shift, including the effect of the substrate/surrounding environment, [49], embedding [54] and also elongation of NPs [28]. In the present case, the polymer surface becomes carbon rich because of the release of volatile species during irradiation, thus altering the surrounding environment of the NPs. A change in the environment of the NPs usually alters the dielectric constant which may give rise to a red shift [55]. It can be seen in the TEM images (Figure 1(d)) that at the higher fluence, partially as well as fully embedded and elongated Au NPs are formed with particle size greater than or equal to 10 nm, which are interestingly surrounded by very small Au NPs of size less than or equal to 5 nm in the carbonaceous matrix. It has been reported that fast relaxation of surface plasmons

(decay into electron-hole pairs) occurs when NPs are very small (less than 5 nm) which can be explained by limitation of the mean free path of the free electrons in these small NPs [56]. When the volume fraction of the NPs becomes high, inter-particle coupling also effects the surface plasmon band which is consistent with the TEM image (Figure 1(d)). Along with this, the surrounding environment can induce additional electronic states at the surface of the NPs, which gives rise to so-called chemical interface damping which also affects the surface plasmon band in such a system embedded with smaller NPs [55,57]. The weak surface plasmon band in the case of the sample irradiated at a fluence of 5×10^{16} ions/cm² is due to the weak response of plasmons and possibly dissipated because of embedded NPs in the carbonaceous matrix [56].

PL Study

PL spectra for thin Au film on PET and irradiated films for different fluences are shown in Figure 4. The PL studies in noble metals started from the work by Mooradian, who assigned the emission around 2.4 eV from a Au film to the direct recombination of the conduction band electrons below the Fermi energy with holes in the *d* band [15]. We observed emission bands for the thin Au film around 2.6 eV and 3.0 eV with a shoulder around 3.1 eV. These match quite well with the experimental peaks reported by Boyd et al. [58] at 2.50 eV and 2.95 eV when excited at 3.50 eV. The small increase in the energies of the peaks as observed in present study can be attributed to the higher energy of excitation used (3.8 eV, or ~ 325 nm). Since the simulations of Boyd et al. [58] identifying these peaks at 2.4 eV and 3.1 eV to be associated with the 6-5*L* and 6-4*L* transitions in the band structure of Au also show that the emission tends to increase slightly with increasing excitation energy (here state 4,5 stand for d-band holes and 6 stands for sp conduction electrons above Fermi level). The observed peak at 2.6 eV is much broader than the peak at 3.0 eV, which may be due to a shoulder at 2.4 eV in the simulated 6-4*L*

emission which was attributed to dispersion of the Fresnel factor by Boyd et al. [58], or to the emergence of additional emission bands made possible at higher excitation energies.

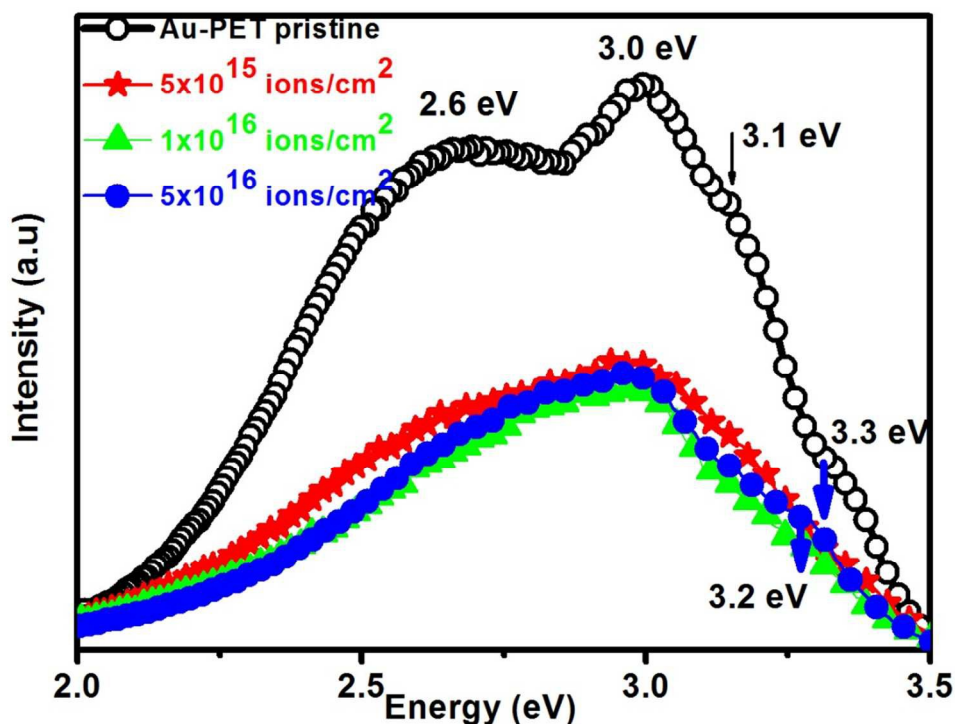


Figure 4: PL spectra of as deposited Au film on PET and films after irradiation with fluences of 5×10^{15} , 1×10^{16} , and 5×10^{16} ions/cm². Here, the PL intensity of the deposited Au film is strongly suppressed (about 100 times) as compared to the irradiated films for clarity of the broadening and comparing the change in the PL peaks induced by ion irradiation at the higher fluences.

The PL spectrum of the sample irradiated at a fluence of 5×10^{15} ions/cm² shows that PL intensity is strongly suppressed (about 100 times) with broadening of the peaks as compared to the luminescence from the unirradiated Au film, although no appreciable change in the peak positions is observed. Boyd et al. [58] considered the possibility of the enhancement of luminescence from roughened surfaces but their results indicate that this effect is restricted to lower energies, with the enhancement effect being essentially quenched at ~ 2.2 eV due to

damping of the plasmon resonances at energies higher than the interband absorption edge of the metal. Therefore such an enhancement is not expected for the emissions observed in the present study where emission bands are observed above 2.0 eV. In some cases, Boyd et al. [58] observed quenching of luminescence due to surface roughness which could not be explained by their model, but which they ascribed to an increased nonradiative recombination rate, perhaps via collisions, associated with the rough surface. The irradiation by 150 keV Ar ions was used by Dollar and Gleiter [59] to produce a large concentration of point defects in Au, which resulted in dislocation loops which were stable in the grains up to 180 °C. Since point defects (such as vacancies and interstitials) and extended defects (such as dislocation loops) can act as non-radiative recombination sites, the strong decrease in luminescence from the irradiated sample in the present case, can be attributed to these defects in addition to possible roughness quenching as described by Boyd et al. [58]. After irradiation at a fluence of 1×10^{16} ions/cm², the broad emission bands around 2.6 and 3.1 eV are suppressed. There is a small decrease in peak intensity at 3.0 eV without any change in the peak position and a shoulder peak around 3.2 eV is observed. These changes can be correlated with a small increase in roughness and also the formation of Au NPs located on the surface as compared to the previous sample where connected nanostructures or spheroid type of nanostructures were formed. The peaks around 3.1 and 3.4 eV have been reported for colloidal NPs (less than 5 nm) and supported Au nanoislands of size more than 10 nm which is consistent with our results as observed in the TEM images at a fluence of 1×10^{16} ions/cm² (Figure 1d) where Au NPs are observed on the modified polymer surface [12]. The UV-Vis spectra also exhibit a strong localized SPR band with a large reflectance dip in the reflection spectra (Figure 3) for the fluence of 1×10^{16} ions/cm². The decrease in intensity of the peak at 2.6 eV in PL spectra after irradiation at a fluence of 1×10^{16} ions/cm² (which seems to be

characteristic of the smooth Au film) also supports the nanostructuring of the film and formation of Au islands. The peak at 3.0 eV is observed to be dominant and a small blue shift (0.1 eV) (as shown with an arrow ↓) with an increase in the intensity is also observed for the peak at 3.3 eV after irradiation at the fluence of 5×10^{16} ions/cm². This is again in accordance with the surface morphology and roughness where surface roughness is slightly increased with the embedded NPs of size around 10 nm surrounded by very small NPs of size less than 5 nm. Theoretically calculated single photon excitation spectra indicate that the peak at ~ 3.3 eV arises because of the 6-4L transition and it appears only in the case of smaller particles (less or equal to 10 nm) as observed in the TEM results (embedded NPs of size less or equal to 5 nm along with some big NPs are formed as shown in Fig. 1d). Whereas, the peak at ~ 3.0 eV arises as a mixture of 6-4L and 6-3X transitions [12,58]. It explains why there is an increase in the intensity of the peak at 3.3 eV with a small blue shift. This small blue shift occurs due to the decrease in the NPs size along with embedding which can be attributed to the strain in the lattice of small Au NPs and elongation of bigger NPs within the carbonaceous matrix.

The Au NPs embedded in the carbonaceous matrix can experience an isotropic pressure from the surrounding matrix resulting in a reduction of average lattice constant and producing compressive strain in the lattice of Au NPs. Similar results have been shown in case of Au NPs embedded in SiO₂ matrix induced by 100 keV Ar ion irradiation [12]. It can be understood from the shifting in the peak position of Au (111) towards the higher angle in the XRD pattern of the sample irradiated at the fluence of 5×10^{16} ions/cm² as compared to others at lower fluences (Figure 5). Thus, the PL spectrum of the sample irradiated at a fluence of 5×10^{16} ions/cm² shows two major peaks above 3.0 eV which correspond to the blue luminescence of Au NPs embedded in the silica matrix as reported by Dhara et al. [12]. As reported by Boyd et al. [58] and discussed

above, the overall decrease in the intensity may be due to an increase in the surface roughness because of the morphological features such as spheroidal and irregular connected nanostructures, spherical NPs and wide size distribution, etc., with increasing ion fluence as well as the defects induced by Ar ion irradiation.

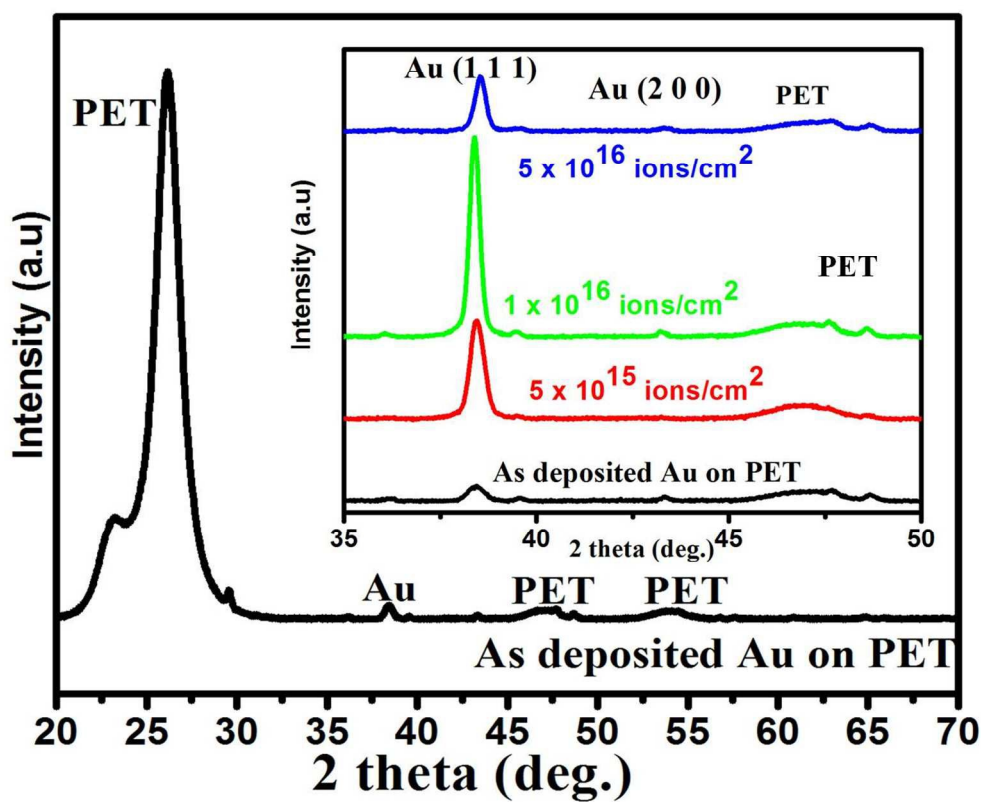


Figure 5: X-ray diffraction pattern of as deposited Au film on PET and films after 150 keVAr ion irradiation at fluences of 5×10^{15} , 1×10^{16} , and 5×10^{16} ions/cm². Inset shows the zoomed image of the region that belongs to Au. PET as shown in XRD patterns of pristine as well as irradiated samples indicate the polymer part of Au/PET systems (shown as PET in the spectra).

At the maximum fluence of 5×10^{16} ions/cm² the surface roughness slightly decreases as compared to that for the fluence of 1×10^{16} ions/cm². The slight increase in the intensity of the peaks is because of the majority of the embedded Au NPs (less than 10 nm) in the carbonaceous matrix (Figure 1(d)) and also because of the amorphous graphitic carbonaceous matrix of the

surrounding environment [49]. The overall mechanism of the blue luminescence as observed in the present case can be attributed to radiative recombination of sp conduction electrons above the Fermi level and d-band holes on the basis of the literature [12,16,58].

3.4. SERS of MO dye adsorbed on Au nanostructured surfaces produced by irradiation

In order to study the SERS on the Au nanostructured surfaces produced by 150 keV Ar ion irradiation of the thin Au film on a PET substrate, MO (an azo-dye molecule), was chosen as a probe to study the Raman activities on these Au nanostructures/PET substrates. Azo-dye molecules are important in optical devices and telecommunications, and have found wide application in reversible optical data storage [26]. Thus, the detection of azo-dye molecules is important from the technological and scientific point of view, in addition to environmental studies because some synthetic dyes are quite toxic and found in waste water that is harmful for society [60]. Very few reports are available including detection of MO on solid SERS substrates [60]. In the present study, MO molecules were adsorbed on PET, thin Au film/PET and Au nanostructured/PET surfaces by immersing the substrates into the aqueous solution of MO and drying. The MO exists in a basic form in aqueous solutions shown in Figure 6 (a). In order to study the effect of the adsorption of MO on the Au nanostructures/PET substrate, the SERS spectra of MO (aqueous solution) on these surfaces were compared with the Raman spectra of MO (aqueous solution) on the PET surface and the normal Raman spectrum of solid MO powder. Figures 6 (b-c) show the normal Raman spectrum of solid MO powder and the Raman spectrum of MO (aqueous solution) on the PET substrate. It can be observed in Figure 6 (c) that the Raman spectrum of MO on the PET polymer substrate has Raman bands which are so weak that they cannot be seen clearly because of the low concentration of the MO molecules in the aqueous solution [61].

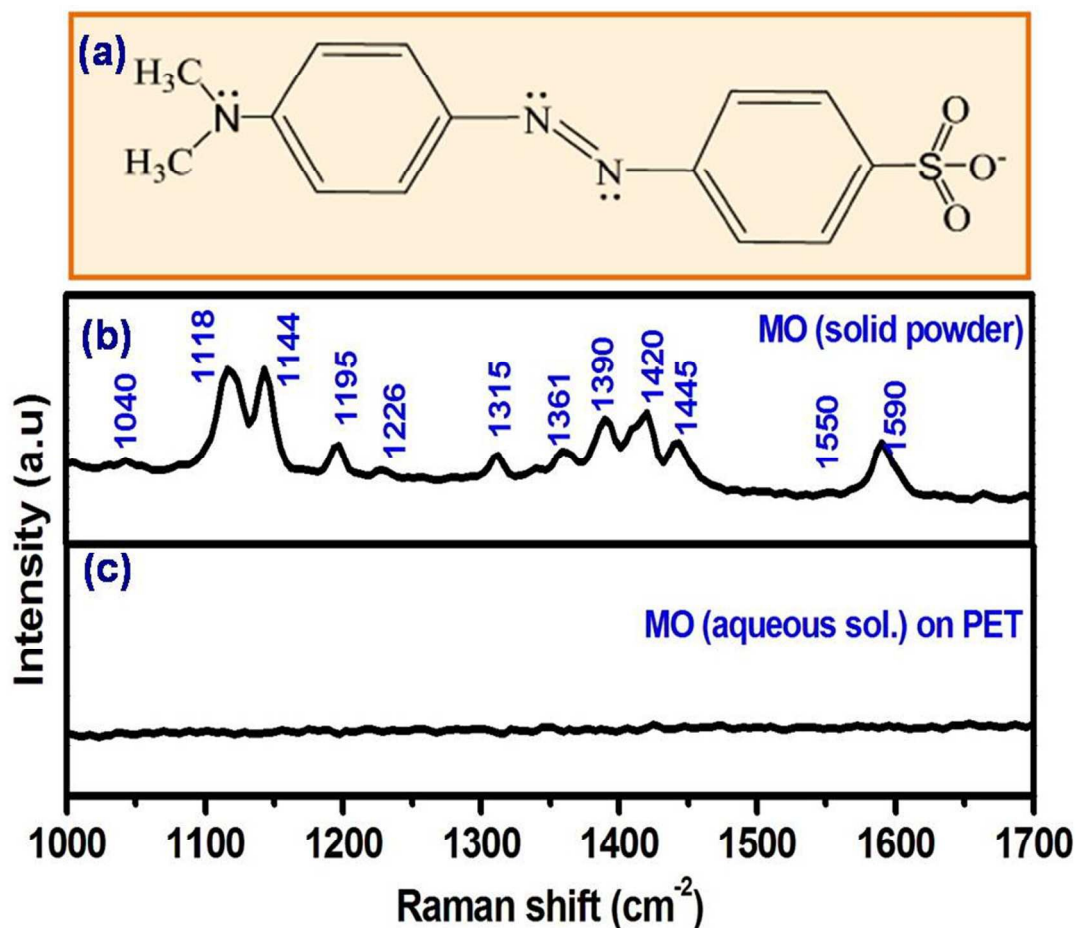


Figure 6: (a) Chemical structure of MO molecule (basic form) in aqueous solution, (b) Raman spectrum of solid MO molecules in powder form (c) Raman spectrum of MO (aqueous solution) on polymer (PET) surface. Raman spectrum of MO powder shows characteristic Raman signals of MO molecules. Raman spectrum of MO on polymer does not show any Raman signals because of low concentration of MO in aqueous solution (For SERS measurement, MO was deposited on the Au nanostructures/PET substrates by immersing them into a 400 mM aqueous solution of MO and were dried prior to the measurement).

The Raman spectrum of the solid MO powder in Fig. 6(b) exhibits strong bands at 1118 cm⁻¹ (C-SO₂-O due to the symmetric stretching motion of SO₃), 1144 cm⁻¹ (Ph-N stretching vibration and aromatic C-C stretching vibration), 1390 cm⁻¹ (C-SO₂-O and N=N stretching), 1420 cm⁻¹ (N=N

stretching vibration) and 1590 cm^{-1} (C=C stretching vibration of both benzene rings). These are comparable with earlier reports [26,60,62,63] and commonly employed as characteristic peaks for evaluating the performance of SERS substrates. Other Raman bands were identified at 1195 cm^{-1} (C-H, C-C and C-N stretching vibrations), 1315 cm^{-1} (S-ring and C-N bending), 1361 cm^{-1} (C-C and Ph-N stretching vibrations), 1445 cm^{-1} (C-C stretching) and 1550 cm^{-1} (C-H bending) [62, 63].

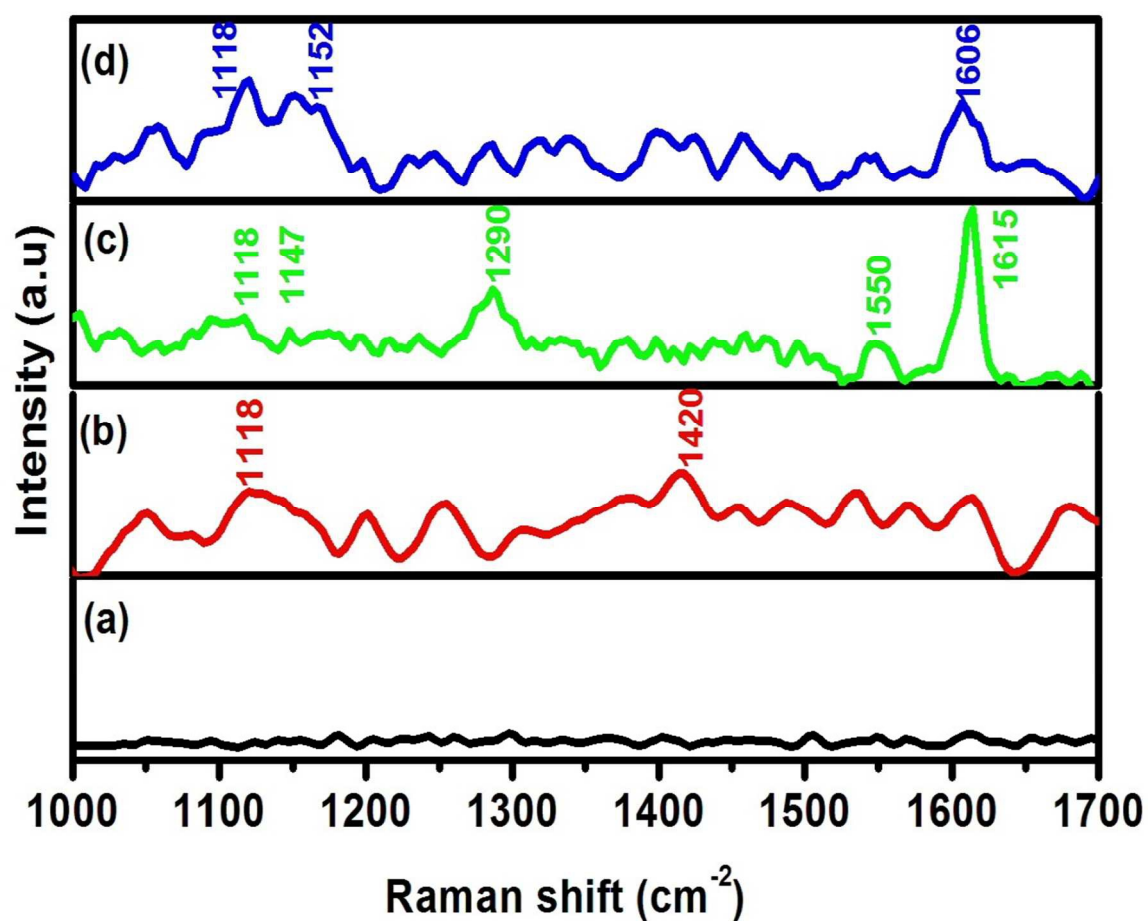


Figure 7: SERS signals of MO on (a) thin Au film/PET and film irradiated with 150 keV Ar ions for fluence of (b) 5×10^{15} , (c) 1×10^{16} , and (d) 5×10^{16} ions/cm².

The SERS activities of the thin Au film and 150 keV Ar ion induced Au nanostructures on a PET substrate for different fluences were studied by measuring SERS of MO (aqueous solution) adsorbed on these surfaces as shown in Figure 7.

The SERS signals are obtained generally when molecules are adsorbed on the metallic surfaces and it can be dominated by electromagnetic or chemical effects [62]. The characteristic bands of MO at 1118, 1420, and around 1600 cm⁻¹ indicate that the MO molecules were adsorbed on the Au nanostructured surfaces (Figure 7). The thin Au film on the PET substrate with insignificant features (AFM images in Figure S1) does not show any significant Raman band in its SERS spectrum (Figure 7(a)). On the other hand, irradiated films with Au nanostructures on the surface show Raman signals of MO molecules with little background noise (Figures 7(b-d)). The Au spheroid nanostructures on the PET substrate after irradiation for the fluence of 5×10^{15} ions/cm² shows very weak SERS signals of MO at 1118 and 1420 cm⁻¹ (Figure 7(b)). Enhanced SERS signals of MO are observed from the surface with spherical Au NPs on the modified PET substrate (at the fluence of 1×10^{16} ions/cm²) indicating that these Au NPs on the PET can be active SERS substrates for the detection of organic molecules. A strong Raman band appears at 1615 cm⁻¹ with a significant shift as compared to the Raman band of solid MO in Figure 6(b), in addition to two other bands at 1290 and 1550 cm⁻¹ (Fig. 7c). The Raman band at 1290 cm⁻¹ is assigned to C-N and N-H stretching vibrations [63]. The enhancement in the intensity of these bands is accompanied by a decrease in the intensity of the band at 1118 and 1144 cm⁻¹ when compared with Raman spectrum of solid MO (Fig. 6(b)). The SERS signals of MO on surface where embedded Au NPs are formed for the fluence of 5×10^{16} ions/cm², show

strong Raman bands at 1118 and 1152 cm^{-1} . Along with these bands, a band also appears at 1606 cm^{-1} accompanied by a significant red shift and decrease in intensity as compared to the band at 1615 cm^{-1} in the case of Au NPs positioned on the surface (compare Figure 7d vs. 7c).

According to the mechanism of SERS, the observed shift in the Raman band and change in intensity are governed by the chemical (i.e. chemisorbed) and electromagnetic effects (i.e. physisorbed), where adsorption orientation of the molecules on the surface also influences SERS signals [61-63]. In the present case the shift in position and change of intensity of Raman signals indicates differing adsorption orientation of MO molecules on the Au NPs positioned on the surface and embedded in the modified PET substrates or Au-C rich polymer composite surface. The connected spheroid-like Au nanostructures show weak interaction towards MO molecules as there is no significant enhancement in the Raman signals (Fig. 7(b)). On the contrary, in the case of Au NPs, the characteristic Raman bands of MO assigned to C=C, C=C stretching (both benzene rings) and C-N stretching vibrations (at 1615 and 1290 cm^{-1} respectively) were enhanced to rather a large extent as compared to other bands appearing in the normal Raman spectrum of solid MO. This indicates a strong interaction between MO molecules and Au NPs on the modified PET surface (Figure 7(c)). The large enhancement of SERS signals can be attributed to localized electric field enhancement of spherical Au NPs and the interparticle surface plasmon coupling effect of isolated but densely distributed spherical NPs [64] as clearly seen in SPR spectra (Figure 3) and TEM images (Figure 1(c)). Yang et al. [64] have demonstrated strong enhancement of SERS signals of malachite green dye on Au nano-needles as compared to a smooth Au film. It was explained by localized electromagnetic field enhancement around the apex of the Au nano-needle (which acts as a SERS 'hot spot' responsible for the enhanced SERS signals) and surface plasmon coupling which arises from the

periodic structures. The strong Raman bands at 1615, 1550 cm^{-1} and the appearance of a new strong band at 1290 cm^{-1} (assigned to C=C (both benzene ring), C-H bending and C-N stretching respectively) indicate that MO molecules may be adsorbed with the benzene ring close to the surface of the Au NPs. In addition, a small enhancement of the band at 1118 cm^{-1} (corresponding to C-SO₂-O) and the absence of the band at 1390 cm^{-1} (corresponding to C-SO₂-O) indicates that the SO₃⁻ group may remain far from the adsorption site on the surface of the Au NPs. These observations from the SERS spectra suggest that MO molecules are adsorbed on the surface with Au NPs/PET lying flat with their molecular plane parallel or near parallel to the surface of Au NPs [62,63]. The Au NPs embedded in the carbon rich PET surface formed after irradiation at the high fluence of 5×10^{16} ions/ cm^2 also show interaction with MO molecules with enhanced Raman signals at 1118, 1152, and 1606 cm^{-1} . The overall SERS signal enhancement of MO molecules in the case of embedded Au NPs is comparatively less than that of Au NPs positioned on the carbonaceous surface because of the weak surface plasmons of embedded Au NPs as discussed in section 3. The enhancement of the Raman band at 1118 cm^{-1} assigned to S-O stretching and a decrease in the band intensity at 1606 cm^{-1} assigned to C=C of benzene rings (shifted by 9 cm^{-1} as compared to when MO adsorbed on Au NPs positioned at the surface) indicate that MO molecules are adsorbed on the Au-C rich polymer composite surface with sulfonate group (SO₃⁻) [63], whereas the benzene ring is located away from the surface. Absence or small enhancement of the SERS signals at 1390 cm^{-1} and 1420 cm^{-1} , both assigned to N=N stretching vibration, also support this assertion. The evolution of a new Raman band at 1152 cm^{-1} which is assigned to C-S stretching [63] also predicts that MO molecules are adsorbed with the SO₃⁻ group on the Au-C rich polymer composite surface. Any contribution from the PET in SERS signals can be ruled out because no Raman signals were observed for MO on the PET, as

can be seen in Figure 6(c). According to the chemical structure of a MO molecule (Figure 6(a)), it can be proposed that MO adsorbs with different orientation on the Au nanostructured surfaces i.e. parallel (or near parallel) or perpendicular (or near perpendicular) when Au NPs are on the surface or embedded within the modified PET substrates respectively, as schematically shown in Figure 8.

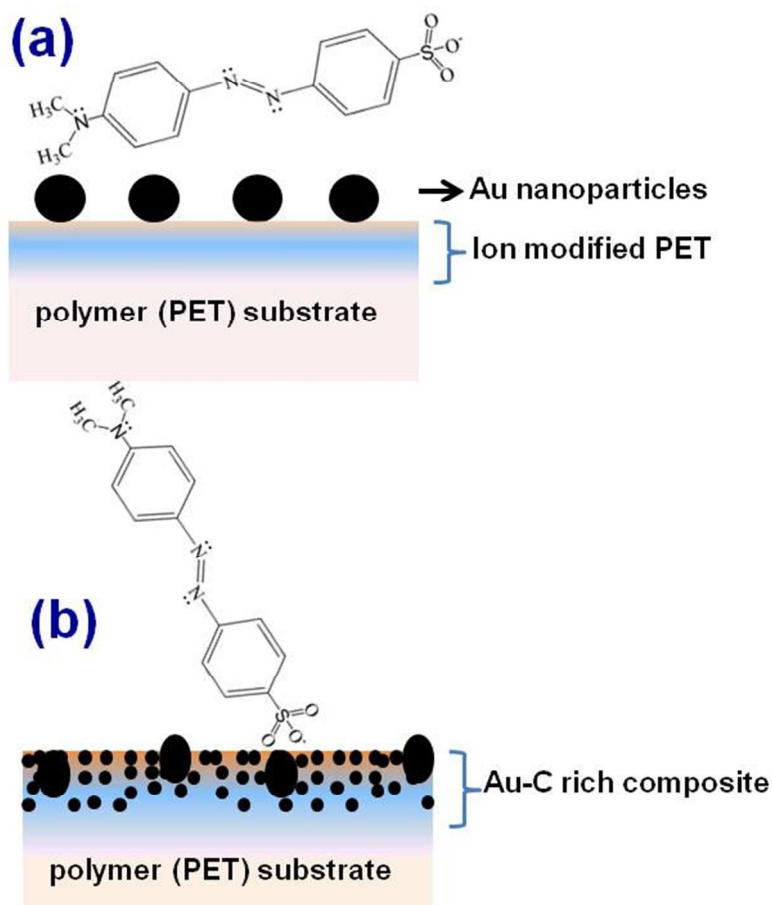


Figure 8: Schematic illustration of the possible different adsorption orientation of MO molecules on the surfaces (a) when Au nanoparticles are on the PET surface (b) when embedded Au nanoparticles are formed i.e. Au-C rich composite surface.

4. Conclusions

In the present study, we investigated (i) the evolution of the surface morphology of a thin Au film on a PET substrate due to 150 keV Ar ion induced thermal spikes and sputtering which resulted in dewetting of the film with subsequent formation of spherical Au NPs, which eventually embedded in the modified PET surface, (ii) the corresponding optical properties obtained by UV-vis diffuse reflection spectroscopy and PL studies, (iii) the chemical modifications in the systems upon irradiation using XPS and (iv) the SERS of MO dye molecules on the Au nanostructured surfaces. Au NPs on the surface and embedded in the carbon rich polymeric matrix were observed where thermodynamic driving forces play a role in the embedding process. These Au NPs on the surface and embedded in the carbonaceous matrix show unique SPR and PL properties as compared to the thin Au film and dewetted (nanospheroid like structures) Au nanostructures on PET. Strong SPR in the case of Au NPs on the surface relative to embedded NPs was observed. The PL properties varied with the surface morphology (i.e. roughness) before and after irradiation and exhibited broad blue luminescence when Au NPs are formed on the surface and became embedded in the matrix. The SERS studies revealed adsorption of MO molecules and enhancement of SERS signals for Au NPs on the surface and when embedded in the modified PET, as compared to for the thin Au film and spheroid like Au nanostructures on the surface. The SERS analyses suggested an adsorption orientation with the molecular plane lying flat (parallel) to the surface when Au NPs are positioned on the surface and perpendicular when embedded Au NPs are formed. The formation of such noble metal NPs on the surface or embedded in the near surface region of the polymer substrate might have

potential applications in solid-state light emitting devices and SERS based sensors for the detection of organic compounds.

Acknowledgement

The Author (JP) would like to acknowledge Materials Science staff at IUAC, New Delhi for AFM/SEM and low ion beam energy irradiation facilities. The author would also like to thank Dr. D. K. Avasthi, A. Tripathi, F. Singh, S. A. Khan, J. Tripathi, Pravin Kumar for their suggestions and encouragement in the beginning of this work. Authors acknowledge Dr. A. Pandey, Dr. M.-M. Duvenhage for their help during handling of the instruments, Dr. Roland Barbosa (ULB, Bruxelles) for XPS measurement, and P/V. Kumar for providing organic molecules. The author would like to acknowledge National Research Foundation (NRF), South Africa for providing all the characterizing facilities such as Raman, UV, PL, XRD, and Raman at UFS used in the experiments. The PL system that was used is supported by the rental pool programme of the National Laser Centre (NLC) of South Africa. The research is also supported by the South African Research Chairs Initiative of the Department of Science and Technology and National Research Foundation of South Africa (Grant Number: 84415). The financial support from the University of the Free State is highly recognized.

References:

1. Prakash, J.; Pivin J. C.; Swart, H. C. Noble metal nanoparticles embedding into polymeric materials: From fundamentals to applications. *Adv. Coll. Interface Sci.* 2015, 226, 187-202.

2. Eichelbaum, M.; Schmidt, B. E.; Ibrahim, H.; Rademann, K. Three-photon-induced luminescence of gold nanoparticles embedded in and located on the surface of glassy nanolayers. *Nanotechnology***2007**, 18, 355702.
3. Deshmukh, Ranjan D.; Compostom, J. R. Direct Observation of Nanoparticle Embedding into the Surface of a Polymer Melt. *Langmuir***2007**, 23, 13169-13173.
4. Kumar, P.; Mathpal, M. C.; Tripathi, A. K.; Prakash, Jai; Agarwal, A.; Ahmad, M. M.; Swart, H. C. Plasmonic resonance of Ag nanoclusters diffused in soda-lime glasses. *Phys. Chem. Chem. Phys.***2015**, 17, 8596-8603.
5. Mathpal, M. C.; Kumar, P.; Kumar, S.; Tripathi, A. K.; Singh, M. K.; Prakash, Jai; Agarwal, A. Opacity and plasmonic properties of Ag embedded glass based metamaterials, *RSC Adv.***2015**, 5, 12555-12562.
6. Schmid, G. Nanoclusters – Building Blocks for Future Nanoelectronic Devices?. *Adv. Eng. Mater.***2001**, 3, 737-743.
7. Biswas, A.; Eilers, H.; Hidden, F.; Aktas, O. C.; Kiran, C. V. S. Large broadband visible to infrared plasmonic absorption from Ag nanoparticles with a fractal structure embedded in a Teflon AF® matrix. *Appl. Phys. Lett.***2006**, 88, 13103.
8. Kreibig, U.; Vollmer, M. *Optical properties of Metal clusters*, Springer, Berlin, 1995.
9. Kim, S. S.; Na, I. S.; Jo, J.; Kim, D. Y.; Nah, Y. C. Plasmon enhanced performance of organic solar cells using electrodeposited Ag nanoparticles, *Appl. Phys. Lett.***2008**, 93, 73307.
10. Choulis, S. A.; Mathai, M. K.; Choong, V. E. Influence of metallic nanoparticles on the performance of organic electrophosphorescence devices, *Appl. Phys. Lett.***2006**, 88, 213503.
11. Nakayama, K.; Tanabe, K.; Harry A. Atwater, Plasmonic nanoparticle enhanced light absorption in GaAs solar cells. *Appl. Phys. Lett.***2008**, 93, 121904.

12. Dhara, S.; Chandra, S.; Magudapathy, P.; Kalavathi, S.; Panigrahi, B. M.; Nair, K.G.M.; Sastry, V. S.; Hsu, C. W.; Wu, C. T.; K. H. Chen; Chen, L. C. Blue luminescence of Au nanoclusters embedded in Silica Matrix. *J. Chem. Phys.* **2004**, 121, 12595-12599.
13. Chen, Li-Yi; Wang, Chia-Wei; Yuan, Zhiqin; Chang, Huan-Tsung. Fluorescent Gold Nanoclusters: Recent Advances in Sensing and Imaging. *Analytical chemistry*, **2015**, 87, 216-229.
14. Khriachtchev, L.; Heikkila, L.; Kuusela, T. Red photoluminescence of gold island films. *Appl. Phys. Lett.* **2001**, 78, 1994.
15. Mooradian, A. Photoluminescence of metals. *Phys. Rev. Lett.* **1969**, 22, 185-187.
16. Wilcoxon, J. P.; Martin, J. E.; Parsapour, F.; Weidenman, B.; Kelley, D. F. Photoluminescence from nanosize gold clusters. *J. Chem. Phys.* **1998**, 108, 9137-9143.
17. Ngoc, L. L T.; Wiedemair, J.; Berg Albert van den; Carlen, Edwin T. Plasmon-modulated photoluminescence from gold nanostructures and its dependence on plasmon resonance, excitation energy, and band structure. *Optics Express*, **2015**, 23, 5547-5564.
18. Eustis S.; El-Sayed, Mostafa A. Why gold nanoparticles are more precious than pretty gold: Noble metal surface plasmon resonance and its enhancement of the radiative and nonradiative properties of nanocrystals of different shapes. *Chem. Soc. Rev.* **2006**, 35, 209–217.
19. Ahn, Wonmi; Taylor, B.; Dall’Asen Analia G.; Roper, D. Keith. Electroless Gold Island Thin Films: Photoluminescence and Thermal Transformation to Nanoparticle Ensembles. *Langmuir*, **2008**, 24, 4174-4184.
20. Zheng, J.; Zhang C.; Dickson, R. M. Highly Fluorescent, Water-Soluble, Size-Tunable Gold Quantum Dots. *Phys. Rev. Lett.*, **2004**, 93, 077402.

21. Farrer, R. A.; Utterfield, F. L.; Chen, V. W.; Fourkas, J. T. Highly efficient multiphoton-absorption-induced luminescence from gold nanoparticles. *Nano Lett.* **2005**, *5*, 1139–42.
22. Yang, Y.; Tanemura, M.; Huang, Z.; Jiang, D.; Li, Zhi-Yuan; Huang, Ying-ping; Kawamura, Go; Yamaguchi, K.; Nogami, M. Aligned gold nanoneedle arrays for surface-enhanced Raman scattering. *Nanotechnology*, **2010**, *21*, 325701.
23. Sivanesan, A.; Witkowska, E.; Adamkiewicz, W.; Dziewit, Ł.; Kaminska, A.; Waluka, J. Nanostructured silver–gold bimetallic SERS substrates for selective identification of bacteria in human. *Analyst*, **2014**, *139*, 1037–43.
24. Lu, Gang; Li, Hai; Liusman, Cipto; Yin, Z.; Wu S.; Zhang, H. Surface enhanced Raman scattering of Ag or Au nanoparticle-decorated reduced graphene oxide for detection of aromatic molecules. *Chem. Sci.*, **2011**, *2*, 1817.
25. Jia, Y. H.; Liao, D. W.; G. Li. Fabrication of Gold Nanoparticle-Embedded Metal–Organic Framework for Highly Sensitive Surface-Enhanced Raman Scattering Detection. *Anal. Chem.* **2014**, *86*, 3955–3963.
26. Si, M.Z.; Kang, Y.P.; Zhang, Z.G. Surface-enhanced Raman scattering (SERS) spectra of Methyl Orange in Ag colloids prepared by electrolysis method. *Appl. Surf. Sci.* **2009**, *255*, 6007–6010.
27. Kelly, K. L.; Coronado, E.; Zhao, L. L.; Schatz, C. C. The optical properties of metal nanoparticles: the influence of size, shape, and dielectric environment. *J. Phys. Chem. B* **2003**, *107*, 668–677.
28. Mishra, Y.K.; Singh, F.; Avasthi, D. K.; Pivin, J. C; Malivoska, D.; Pippel, E. Synthesis of elongated Au nanoparticles in silica matrix by ion irradiation. *Appl. Phys. Lett.* **2007**, *91*, 63103.

29. Prakash, Jai; Tripathi, A.; Rigato, V.; Pivin, J. C.; Tripathi, J.; Chae, K. H.; Gautam, S.; Kumar, P.; Asokan, K.; Avasthi, D. K. Synthesis of Au nanoparticles at the surface and embedded in carbonaceous matrix by 150 keV Ar ion irradiation. *J. Phys. D: Appl. Phys.* **2011**, 44, 125302.
30. Prakash, J.; Tripathi, A.; Gautam, S.; Chae, K. H.; Song, J.; Rigato, V.; Tripathi, J.; Asokan, K. Phenomenological understanding of dewetting and embedding of noble metal nanoparticles in thin films induced by ion irradiation. *Mat. Chem. Phys.* **2014**, 147, 920-924.
31. Prakash, J.; Tripathi, A.; Pivin, J. C.; Tripathi, J.; Chawla, A. K.; Chandra, R.; Kim, S. S.; Asokan, K.; Avasthi, D. K. Study on synthesis of magnetic nanocomposite (Ni-Teflon) by swift heavy ion beam mixing. *Adv. Mat. Lett.* **2011**, 2, 71-75.
32. Prakash, J.; Tripathi, A.; Lakshmi, GVBS; Rigato, V.; Tripathi, J.; Avasthi, D. K. Synthesis of Ag nanoparticles on polymer surface: 150 keV Ar ion irradiation. *Adv. Mat. Lett.* **2013**, 4, 408-412.
33. Biswas, A.; Avasthi, D. K.; Fink, D.; Kanzow, J.; Schürmann, U.; Ding, S. J.; Aktas, O. C.; Saeed, U.; Zaporozhchenko, V.; Faupel, F.; Gupta, R.; Kumar, N. Nanoparticle architecture in carbonaceous matrix upon swift heavy ion irradiation of polymer-metal nanocomposites. *Nucl. Instr. Meth. Phys. Res. B* **2004**, 217, 39-50.
34. Singhal, R.; Kabiraj, D.; Kulriya, P. K.; Pivin, J. C.; Chandra, R.; Avasthi, D. K. Blue-Shifted SPR of Au nanoparticles with ordering of carbon by dense ionization and thermal treatment. *Plasmonics*, **2013**, 8, 295-305.
35. Hu X.; Cahill D. G.; Averbach R. S. Nanoscale pattern formation in Pt thin films due to ion beam induced dewetting. *Appl. Phys. Lett.* **2000**, 76, 3215-3217.

36. Grochowska, K.; Śliwiński, G.; Iwulska, A.; Sawczak, M.; Nedyalkov, N.; Atanasov P.; Obara, G.; Obara, M. Engineering Au Nanoparticle Arrays on SiO₂ Glass by Pulsed UV Laser Irradiation. *Plasmonics*, **2013**, 8, 105–113.
37. Hu, X.; Cahill, D. G.; Averback, R. S. Dewetting and nanopattern formation of thin Pt films on SiO₂ induced by ion beam irradiation. *J. Appl. Phys.* **2001**, 89, 7777–7783.
38. Meng, X.; Shibayama, T.; Yu, R.; Takayanagi, S. Seiichi Watanabe, Microstructure analysis of ion beam-induced surface nanostructuring of thin Au film deposited on SiO₂ glass. *J. Mat. Sci.* **2013**, 48, 920-928.
39. Hu, X.; Cahill, D. G.; Averback, R. S.; Birtcher, R. C. In-situ transmission electron microscopy study of irradiation induced dewetting of ultrathin Pt films. *J. Appl. Phys.* **2003**, 93, 165-169.
40. Hu, X.; Cahill, D. G.; Averback, R. S.; Burrowing of Pt nanoparticles into SiO₂ during ion-beam irradiation, *J. Appl. Phys.* **2002**, 92, 3995-4000.
41. Calliari, L.; Speranza, G.; Minati, L.; Micheli, V.; Baranov, A.; Fanchenko, S. Composition and structure of a-C:Au nanocomposites obtained by physical vapour deposition. *Appl. Surf. Sci.* **2008**, 255, 2214-2218.
42. Mohapatra, S.; Mishra, Y. K.; Avasthi, D. K.; Kabiraj, D.; Ghatak, J.; Verma, S. Synthesis of gold silicon core shell nanoparticles with tunable localized surface Plasmon response. *Appl. Phys. Lett.* **2008**, 92, 103105.
43. Takahiro, K.; Oizumi, S.; Terai, A.; Kawatsura, K.; Tsuchiya, B.; Nagata, S.; Yamamoto, S.; Naramoto, H.; Narumi, K.; Sasase, M. Core level and valence band photoemission spectra of Au clusters embedded in carbon. *J. Appl. Phys.* **2006**, 100, 84325.

44. Thune, E.;Carpene, E.; Sauthoff, K.; Seibt, M.; Reinke, R. Gold nanoclusters on amorphous carbon synthesized by ion beam deposition. *J. Appl. Phys.***2005**, 98, 34304.
45. Prakash, Jai;Tripathi, A.;Khan, S. A.;Pivin, J. C.;Singh, F. ;Tripathi, J.; Kumar, S.; Avasthi, D. K. Ion beam induced interface mixing of Ni on PTFE bilayer system studied by quadrupole mass analysis and electron spectroscopy for chemical analysis.*Vacuum*,**2010**, 84, 1275-1279.
46. Lakshmi, GBVS;Prakash, J.; Khan, S. A.; Siddiqui, A. M.;Zulfeqar, M.Modifications Induced by Swift Heavy Ion Beam of 60 MeV Si⁵⁺ in Poly (3-octylthiophene). *Sci. of Adv. Mat.***2012**, 4, 1024-1030.
47. Marletta, G.;Catalano, S. M.; Pignataro, S.Chemical reactions induced in polymers by keV ions, electrons and photons.*Surf. Interf. Anal.* **1990**, 16, 407-411.
48. Doren, A.; Genet, M. J.;Rauxhet, P. G. Analysis of poly(ethylene terephthalate) (PET) by XPS.*Surf. Sci. Spectra*, **1994**, 3, 337.
49. Gaspar, D.;Pimentel, A. C.;Mateus, T.; Leitao, J. P.;Soares, J.;Falcao, B. P.; Arau, A.; Vicente, A.; Filonovich, S. A.;Aguas, H.; Martins,R.; Ferreira, I. Influence of the layer thickness in plasmonic gold nanoparticles produced by thermal evaporation. *Sci. Reports*, **2013**, 3, 1469.
50. El-Sayed, M. A. Some interesting properties of metals confined in time and nanometre space of different shapes. *Accounts of chemical research* **2001**, 34, 257-264.
51. Halas, N. J.;Lal, S.;Chang, W. S.;Link, S.;Nordlander, P. Plasmonic in strongly coupled metallic nanostructures. *Chem. Rev.***2011**, 111, 3913-3961.
52. Jana, Nikhil R.,Gearheart, L.;Obare, Sherine O.;Murphy, Catherine J. Anisotropic Chemical Reactivity of Gold Spheroids and Nanorods.*Langmuir*, **2002**, 18, 922-927.

53. Sun, H.; Yu, M.; Wang, G.; Sun, X.; Lian, J. Temperature-dependent morphology evolution and surface plasmon absorption of ultrathin gold island films. *J. Phys. Chem. C* **2012**, 116, 9000-9008.
54. Karakouz, T.; Tesler, A. B.; Sannomiya, T.; Feldman, Y.; Vaskevich, A.; Rubinstein, I. Mechanism of morphology transformation during annealing of nanostructured gold films on glass. *Phys. Chem. Chem. Phys.*, **2013**, 15, 4656-4665.
55. Hendrich, C.; Bosbach, J.; Stietz, F.; Hubenthal, F.; Vartanyan, T.; Trager, F. Chemical interface damping of surface plasmon excitation in metal nanoparticles: a study by persistent spectral hole burning. *Appl. Phys. B* **2003**, 76, 869-875.
56. Mishra, Y. K.; Mohapatra, S.; Avasthi, D. K.; Kabiraj, D.; Lalla, N. P.; Pivin, J. C.; Sharma, H.; Kar, R.; Singh, N. Gold-Silica nanocomposites for the detection of human ovarian cancer cells; a preliminary study. *Nanotechnology* **2007**, 18, 345606.
57. Hovel, H.; Fritz, S.; Hilger, A.; Dreibig, U.; Vollmer, M.; Width of cluster plasmon resonance: Bulk dielectric functions and chemical interface damping. *Phys. Rev. B* **1993**, 48, 178-185.
58. Boyd, G. T.; Yu, Z. H.; Shen, Y. R. Photo induced luminescence from the noble metals and its enhancement on roughened surfaces, *Phys. Rev. B* **1986**, 33, 7923-7936.
59. Dollar, M.; Gleiter, H.; Point defect annihilation in grain boundaries in gold. *Scripta Metallurgical*, **1985**, 19, 481-484.
60. Wu, M.-C.; Lin, M.-P.; Chen, Sh-W.; Lee, P.-H.; Li, J.-H.; Su, W.-F. Surface enhanced Raman scattering substrate based on a Ag coated monolayer array of SiO₂ spheres for organic dye detection. *RSC Adv.* **2014**, 4, 10043-10050.

61. Xiao, G.-N.; Man, S.-Q. Surface enhanced Raman scattering of methylene blue adsorbed on cap shaped silver nanoparticles *Chem. Phys. Lett.* **2007**, 447, 305-309.
62. Zhang, A.; Fang, Y. Adsorption orientations and interactions of methyl orange on negatively and positively charged colloidal silver particles, *J. Colloid. Interf. Sci.* **2007**, 305, 270-274.
63. Zhang, A.; Fang, Y. Influence of adsorption orientation of methyl orange on silver colloids by Raman and fluorescence spectroscopy: pH effect. *Chem. Phys.* **2006**, 331, 55-60.
64. Yang, Y.; Tanemura, M.; Huang, Z.; Jiang, C.; Li, Z.-Y.; Huang, Y.-P.; Kawamura, G.; Yamaguchi, K.; Nogami, M. Aligned gold nanoneedle arrays for surface-enhanced Raman scattering. *Nanotechnology*, **2010**, 21, 325701.